

Systematic investigation of terahertz-induced excitonic Rabi splitting

M. Teich,^{*} M. Wagner, D. Stehr, H. Schneider, and M. Helm

Institute of Ion Beam Physics and Materials Research, Helmholtz-Zentrum Dresden-Rossendorf, P.O. Box 510119, 01314 Dresden, Germany

C. N. Böttge, A. C. Klettke, S. Chatterjee, M. Kira, and S. W. Koch

Department of Physics and Material Sciences Center, Philipps-Universität Marburg, Renthof 5, 35032 Marburg, Germany

G. Khitrova and H. M. Gibbs[†]

College of Optical Sciences, The University of Arizona, 1630 East University Boulevard, Tucson, Arizona 85721, USA

(Received 18 January 2013; revised manuscript received 28 February 2014; published 17 March 2014)

Weak near-infrared and strong terahertz excitation are applied to study excitonic Rabi splitting in (GaIn)As/GaAs quantum wells. Pronounced anticrossing behavior of the split peaks is observed for different terahertz intensities and detunings relative to the intra-excitonic heavy-hole $1s-2p$ transition. At intermediate to high electric fields the splitting becomes highly asymmetric and exhibits significant broadening. A fully microscopic theory is needed to explain the experimental results. Comparisons with a two-level model reveal the increasing importance of higher excitonic states at elevated excitation levels.

DOI: [10.1103/PhysRevB.89.115311](https://doi.org/10.1103/PhysRevB.89.115311)

PACS number(s): 78.67.De, 42.50.Hz, 73.21.Fg, 78.40.Fy

I. INTRODUCTION

The resonant optical polarization in semiconductor quantum wells (QWs) is often referred to as *coherent excitons* [1] which can be classified using the well-known hydrogen quantum numbers. With the help of additional terahertz (THz) excitation, one can couple the different exciton states and, in particular, induce transitions between the $1s$ and $2p$ states [1–8]. In this connection, strong resonant quasi-cw THz excitation of the $1s-2p$ transition leads to Rabi splitting [9]. Pronounced anticrossing behavior was observed by Wagner *et al.* [10] when detuning the THz frequency from the $1s-2p$ transition. These effects were explained within the rotating-wave approximation (RWA) which already predicts dressed states.

A number of theoretical investigations have previously been reported on the effect of a strong THz field on, e.g., the excitonic absorption [11]. The Autler-Townes splitting and sideband generation for excitonic resonances in QWs were discussed theoretically using the RWA [12,13]. However, a more extensive framework of a fully microscopic theory has already been developed [1,7,14] to fully include non-RWA, ponderomotive, and multiphoton-ionization contributions which are needed to describe extreme nonlinear THz excitation.

In addition, Maslov *et al.* analyzed the quantum-confined Stark effect in the presence of a THz field oriented in the growth direction [15]. More detailed studies concerning the combination of an ac and dc field were computed by Mi *et al.* [16]. The interplay between the dynamic Franz-Keldysh and the ac-Stark effect were also discussed by Zhang *et al.* [17]. Yan *et al.* investigated the interplay between the ac-Stark effect and dynamical localization in a semiconductor superlattice [18]. Rabi-splitting effects were also observed using strong THz single-cycle pulses [19]. In addition to the splitting, also pronounced resonance broadening and induced

absorption effects were observed, which could be attributed to the excitation of excitonic states with high quantum numbers and THz-induced exciton ionization.

In this paper, we present a systematic investigation that is intended to fill the gap between the earlier studies and allow us to quantify the limitations of the two-level analysis that includes only the excitonic $1s-2p$ transition. For this purpose, we use the temporally long (31 ps) THz pulses of a free-electron laser (FEL) that are spectrally sufficiently narrow to enable us to study detuning effects from the $1s-2p$ -transition frequency. Furthermore, we use a sample with larger separation between heavy- and light-hole energies than used in Ref. [10]. We record the THz-induced changes in the near-infrared (NIR) absorption spectrum for weak (1.2 kV/cm) to high THz fields up to 6 kV/cm. Since a two-level approximation (2LA) is expected to explain only some aspects of the investigation, it is interesting to determine its validity range. As in Ref. [19], we use a microscopic theory [1,7,14] for the analysis and we compare the results to a 2LA where we restrict the treatment to the excitonic $1s$ and $2p$ states. We quantify when and how a 2LA deviates from the experimental observations, whereas the fully microscopic theory explains the experiments.

II. EXPERIMENTAL SETUP

Figure 1 illustrates the experimental setup which is a two-beam collinear configuration for THz- and NIR-excitation spectroscopy. The setup allows the simultaneous excitation of the sample with weak, broadband NIR and strong, narrow-band THz light. Apart from the sample used, it is the same setup as in Ref. [20]. Broadband NIR light is generated in a 12-fs Ti:sapphire-laser oscillator with a repetition rate of 78 MHz. The repetition rate is reduced by an acousto-optical pulse picker to the 13 MHz of the free-electron laser (FEL) at the Helmholtz-Zentrum Dresden-Rossendorf. Both beams are synchronized with a timing jitter of 1-2 ps; the delay can be adjusted using a phase shifter. The full width at half maximum (FWHM) of the FEL pulses is about a factor of 100 smaller than its photon energy, i.e., for a photon energy of 6.8 meV

^{*}m.teich@hzdr.de

[†]Deceased.

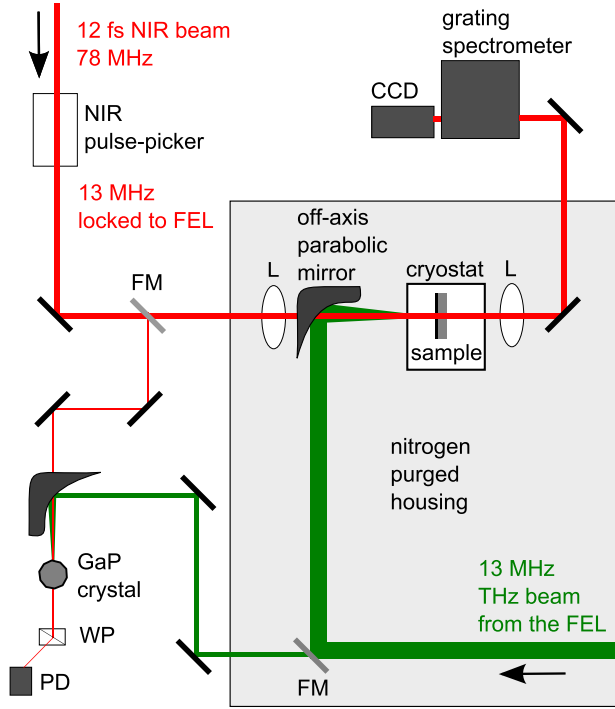


FIG. 1. (Color online) Schematic experimental geometry. FM: flip mirror; L: lens; WP: Wollaston prism; PD: photodiode.

(resonant detuning) we measure 0.06 meV FWHM yielding 31 ps FEL pulses. The FEL pulse duration is determined by Fourier transforming the FEL spectrum and confirmed by a cross-correlation measurement in a 300 μm thick GaP crystal using intensity-based electro-optic sampling with a single Si photodiode [21]. The investigated multiple quantum-well sample DBR42 contains 20 8 nm $\text{Ga}_{0.94}\text{In}_{0.06}\text{As}$ QWs separated by 92 nm GaAs barriers grown on a GaAs substrate [22]. Unlike in the sample analyzed in Ref. [10], the light hole is energetically more separated from the heavy hole.

III. THEORY

We use a systematic many-body theory to determine the polarization dynamics self-consistently via the Maxwell–semiconductor Bloch equations (SBEs) [23,24] with additional terms for the THz interaction [1,7], based on the cluster-expansion approach [25]. This theory has already been applied, e.g., in Ref. [19], to analyze THz experiments. Therefore, we review here only the basic ideas. For optical (or NIR) light propagating along the z direction, the wave equation

$$\left(\frac{\partial^2}{\partial z^2} - \frac{n(z)^2}{c^2} \frac{\partial^2}{\partial t^2} \right) E_{\text{opt}}(z,t) = \mu_0 \delta(z) \frac{\partial^2 P}{\partial t^2} \quad (1)$$

describes the properties of classical light. In this connection, the optical field E_{opt} is changed by the macroscopic polarization P in the quantum well at position z . The vacuum speed of light is denoted by c , $n(z)$ is the refractive-index profile of the sample, and the vacuum permeability is μ_0 . An analytic solution for the transmitted optical field is given by [1]

$$E_T(z,t) = E_{\text{in}}(z,t) - \mu_0 \frac{c}{2n} \frac{\partial}{\partial u} P(u) \Big|_{u=t-|nz|/c}, \quad (2)$$

where $E_{\text{in}}(z,t)$ is the incoming laser pulse that approaches the QW. In the frequency domain, this yields

$$E_T(\omega) = E_{\text{in}}(\omega) + i\mu_0 \frac{c}{2n} \omega P(\omega). \quad (3)$$

From that, we obtain the transmission which is defined as $T = |E_T/E_{\text{in}}|^2$, eventually compared with the experimental spectrum. The THz-induced changes in T originate from the macroscopic polarization P which is a sum of the microscopic polarizations $P_{\mathbf{k}}$, weighted by the dipole-matrix element d_{cv} :

$$P = \frac{d_{cv}}{S} \sum_{\mathbf{k}} P_{\mathbf{k}} + \text{c. c.}, \quad (4)$$

where c. c. stands for the complex conjugation and $\hbar\mathbf{k}$ is the carrier momentum. The dynamics of the polarization follow from the semiconductor Bloch equation [24]:

$$\begin{aligned} i\hbar \frac{\partial}{\partial t} P_{\mathbf{k}} = & \left(\epsilon_{\mathbf{k}} - \mathbf{j}_{\mathbf{k}} \cdot \mathbf{A}_{\text{THz}} + \frac{|e|^2}{2\mu} \mathbf{A}_{\text{THz}}^2 \right) P_{\mathbf{k}} \\ & - (1 - f_{\mathbf{k}}^e - f_{\mathbf{k}}^h) \left(d_{cv} E_{\text{opt}} + \sum_{\mathbf{k}'} V_{\mathbf{k}-\mathbf{k}'} P_{\mathbf{k}'} \right) \\ & + \Gamma_{\mathbf{k},\text{phon}}^{vc} + \Gamma_{\mathbf{k},\text{Coul}}^{vc}. \end{aligned} \quad (5)$$

We observe that $P_{\mathbf{k}}$ becomes coupled with electron–(hole) densities $f_{\mathbf{k}}^{e(h)}$. However, weak optical light creates only low densities ($f_{\mathbf{k}}^{e(h)} \ll 1$), which modifies the phase-filling factor $(1 - f_{\mathbf{k}}^e - f_{\mathbf{k}}^h)$ only minutely. Therefore, the time evolution of the densities is neglected for the dilute excitations reached in our experiment.

Structurally, the Rabi frequency $d_{cv} E_{\text{opt}}$ generates the microscopic polarization whereas the Coulomb interaction $V_{\mathbf{k}-\mathbf{k}'}$ renormalizes it. In this connection, $\epsilon_{\mathbf{k}}$ determines the kinetic energy of an electron–hole pair, associated with $P_{\mathbf{k}}$. The THz vector potential \mathbf{A}_{THz} induces transitions via the THz-current matrix element $\mathbf{j}_{\mathbf{k}}$ and renormalizes the kinetic energy via the ponderomotive current $\frac{|e|^2}{2\mu} \mathbf{A}_{\text{THz}}^2$. The reduced electron–hole mass is $\mu = m_e m_h / (m_e + m_h)$; the effective masses of the electrons and holes are 0.0665 m_0 and 0.236 m_0 where m_0 is the bare electron mass.

The higher-order correlations between the carriers lead to energy renormalizations and to dephasing of the polarization due to the scattering and phonon creations. They are described microscopically by [1]

$$\begin{aligned} \Gamma_{\mathbf{k},\text{Coul}}^{vc} = & \sum_{\mathbf{k}', \mathbf{q} \neq 0, \lambda} V_{\mathbf{q}} [c_{v,\lambda,\lambda,c}^{\mathbf{q},\mathbf{k}',\mathbf{k}} - (c_{c,\lambda,\lambda,v}^{\mathbf{q},\mathbf{k},\mathbf{k}'})^*], \\ \Gamma_{\mathbf{k},\text{phon}}^{vc} = & \sum_{\mathbf{q}} (\Delta \langle Q_{c,\mathbf{q}} a_{v,\mathbf{k}}^\dagger a_{c,\mathbf{k}-\mathbf{q}} \rangle - \Delta \langle Q_{v,\mathbf{q}} a_{v,\mathbf{k}-\mathbf{q}}^\dagger a_{c,\mathbf{k}} \rangle). \end{aligned} \quad (6)$$

The $c_{\lambda,\lambda',v,v'}$ denote coherent carrier correlations and the terms with $Q^{(\dagger)}$ describe the correlations at the creation or annihilation of phonons.

These equations can be described both in $\mathbf{p} \cdot \mathbf{A}$ and $\mathbf{x} \cdot \mathbf{E}$ gauge [26], with the $\mathbf{p} \cdot \mathbf{A}$ gauge leading to numerically easier equations. In linear response, both yield

$$\Gamma_{\mathbf{k},\text{phon}}^{vc} + \Gamma_{\mathbf{k},\text{Coul}}^{vc} = \sum_{\mathbf{k}'} \Gamma_{\mathbf{k},\mathbf{k}'} P_{\mathbf{k}'}, \quad (7)$$

describing the diffusive scattering of $P_{\mathbf{k}}$ into $P_{\mathbf{k}'}$. The Coulomb and phonon interactions account for correct momentum exchange in the scattering process. Since this process is the result of the electron-hole excitation in the system, it is often referred to as *excitation-induced dephasing* (EID) [1,25,27–32]. The effects of EID profoundly alter the many-body system and lead to state-dependent broadening of excitonic resonances for elevated densities. This diffusive character redistributes the microscopic polarizations and leads to a decay of the polarizations within a few picoseconds.

The homogeneous solution of the differential equation for the polarization defines the Wannier equation [1],

$$\epsilon_{\mathbf{k}} \phi_{\lambda}^{\mathbf{R}}(\mathbf{k}) - (1 - f_{\mathbf{k}}^e - f_{\mathbf{k}}^h) \sum_{\mathbf{k}'} V_{\mathbf{k}-\mathbf{k}'} \phi_{\lambda}^{\mathbf{R}}(\mathbf{k}') = E_{\lambda} \phi_{\lambda}^{\mathbf{R}}(\mathbf{k}). \quad (8)$$

We can use the resulting right-handed eigenstates $\phi_{\lambda}^{\mathbf{R}}(\mathbf{k})$ to project the polarizations $P_{\mathbf{k}}$ into the excitonic basis via $P_{\mathbf{k}} = \sum_{\lambda} p_{\lambda} \phi_{\lambda}^{\mathbf{R}}(\mathbf{k})$ with exciton state λ [1]. This allows us to use the more intuitive picture of the hydrogen atom to distinguish the different components of the polarization: In this picture, optical fields couple only to exciton states with an s -like symmetry. The THz light redistributes existing polarization while changing the orbital quantum number by ± 1 . The selection rules determine that the optical light creates mostly $1s$ polarization, while the THz light transfers $1s$ polarization into $2p$ polarization and higher polarizations. We follow this dynamics by computing the squared transition amplitudes $|p_{\lambda}|^2$ that define the probability to find polarizations at exciton state λ .

The EID effects can also be systematically mapped into the exciton basis. One simply projects Eq. (7) with $\phi_{\lambda}^{\mathbf{R}}(\mathbf{k})$ that gives a different dephasing constant γ_{λ} for each p_{λ} component. As shown in Ref. [1], we find that exciton states beyond $1s$ show dephasing constants γ_{λ} that are a few times larger than the $1s$ -exciton-state dephasing γ_{1s} . In contrast, a genuine decay given by a constant dephasing γ which is equal for all states cannot satisfy general conservation laws such as total-polarization conservation [1]. The importance and effects of EID on the computed transmission spectra are discussed in more detail in Sec. IV A.

Another advantage of the projection of the SBE into the exciton basis is that one can check whether restricting the simulation to a two-level model by taking into account only the $1s$ and $2p$ state influences the THz-induced effects. More specifically, this can be implemented by taking into account only the $1s$ and $2p$ states. We will use this later in the paper when we study the influence of the higher exciton states and of the continuum by performing the simulations with only the $1s$ and $2p$ states. Comparing the results with those of the full analysis allows us to identify the influence of the higher excitonic states on the spectrum.

IV. RESULTS AND ANALYSIS

An overview of the measured experimental spectra plotted as $-\log(\text{transmission})$ is given in Fig. 2 for a THz-photon energy (a) above, (b) near, and (c) below the $1s$ – $2p$ -transition energy. The peak field strength in kV/cm is given in the legend. For better visibility, the spectra are vertically shifted. In all cases, THz pumping leads to bleaching for low THz

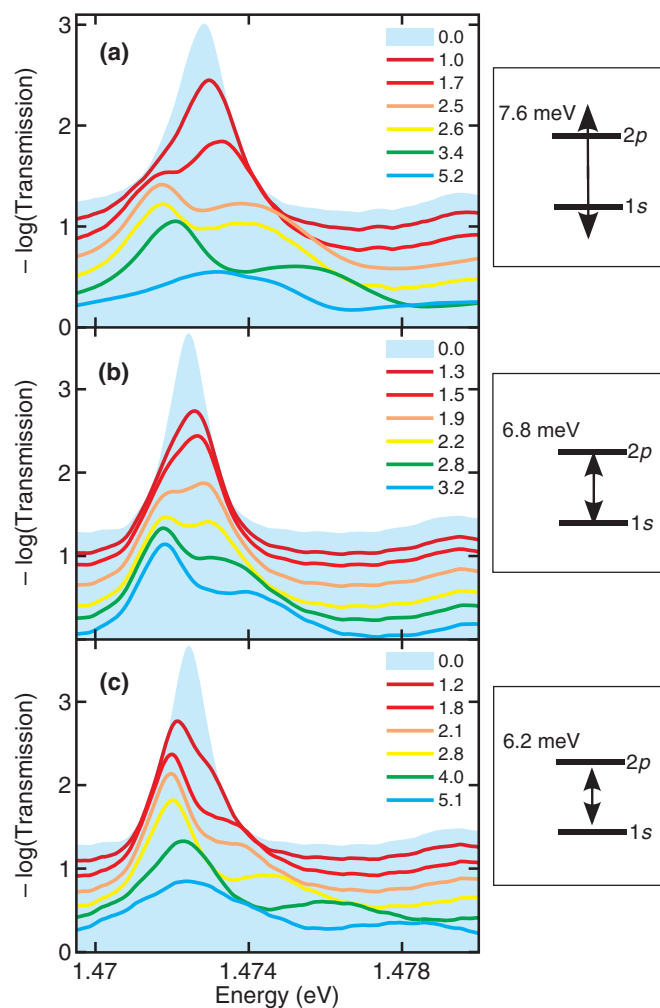


FIG. 2. (Color online) Experimental absorption data [$-\log(\text{transmission})$] for different THz-peak field strengths (in kV/cm) and THz-photon energy (a) above (7.6 meV), (b) near (6.8 meV), and (c) below (6.2 meV) $1s$ – $2p$ resonance.

intensities, then to Rabi splitting from medium intensities on and, in Figs. 2(a) and 2(b), to a reversal of the peak heights. For high intensities, both peaks are bleached but the left peak is higher than the right peak.

We use the microscopic theory [1,7,14,19,24] (semiconductor Bloch equations including THz interaction) to treat the light-matter interaction self-consistently. For the THz interaction, we do not employ the RWA, but fully include the counter-rotating terms. Besides inserting the material parameters appropriate for the sample used in the present study, we additionally evaluate the equations in the limit of the two-level approximation (2LA) where we only include the excitonic $1s$ and $2p$ states but keep all other parameters the same as in the full analysis. This allows us to quantify how and when the 2LA analysis deviates from experiments.

A. Determining excitation-induced dephasing and inhomogeneous broadening

In principle, the EID modifies the QW absorption to a degree that one can determine the precise exciton-versus-plasma

configuration in the excited QW, as demonstrated in Ref. [25]. This can be deduced by comparing the measured excitonic absorption spectrum with a large set of spectra computed as a function of many-body configurations. Here, we want to investigate THz-induced changes in the optical absorption when the system is initially dominated by $1s$ excitons at dilute excitation levels, as discussed in Sec. III. In this situation, the EID mainly broadens the $1s$ resonance by γ_{1s} without generating major asymmetries. The principal effect of EID is reflected in the fact that γ_{1s} is roughly two times smaller than the other γ_λ , as shown in Ref. [1].

Therefore, we fit the EID parameters from the experiment using a systematic procedure instead of extracting the exact many-body state. Since the transmission resonance at the $1s$ -exciton energy is well separated from the other bound states, its width is directly influenced by γ_{1s} . However, the sample has also disorder that yields additional inhomogeneous broadening. We will next deduce γ_{1s} and inhomogeneous broadening by matching the half width of the measured transmission resonance with the computed one. Once γ_{1s} is known, γ_λ of other exciton states is given by $\gamma_\lambda = 2\gamma_{1s}$ as discussed above.

Figure 3(a) shows the measured transmission spectrum (shaded area). To deduce γ_{1s} , we choose the half width of the computed spectrum to match with the experiment. The result without inhomogeneous broadening and $\gamma_{1s} = 0.5$ meV is shown as a dashed line. This result reproduces the measured $1 - T$ resonance peak rather well while it is significantly higher at the tails of the resonance. In other words, the measured $1 - T$ spectrum decays much faster than the Lorentzian matching its width, which indicates that this sample has detectable inhomogeneous broadening.

In general, sample growth is always associated with imperfections and irregularities that produce, e.g., monolayer fluctuations. As a result, the QW shows a distribution of $1s$ energies which induces additional broadening due to energetic spreading of the $1s$ resonance [33]. These variations of the well widths eventually lead to fluctuations of the confinement energies, broadening the overall exciton resonance inhomogeneously. Studying the exact form of such inhomogeneous effects is clearly not the main focus of this paper. Therefore, we use an alternative approach to model disorder effects: Since our sample contains 20 QWs, we can generate an ensemble of $1s$ resonances by assuming that each QW is homogeneous but has a different energy than the other QWs. With this model, we account for well-width fluctuations which usually arise for typical QWs [33]. In more detail, we have shifted the $1s$ energies of each QW by $[-0.60, -0.45, -0.30, -0.20, -0.05, -0.04, -0.03, -0.02, -0.01, 0.00]$ meV for QWs 1–10 and by $[0.00, 0.01, 0.02, 0.03, 0.04, 0.05, 0.20, 0.30, 0.45, 0.60]$ meV for QWs 11–20.

With this setup, we need $\gamma_{1s} = 0.3$ meV to fit the half width of the experimental $1 - T$ spectrum; this theory result is shown as a solid line in Fig. 3(a). While the homogeneously broadened result (dashed) fails to describe the experiment (shaded area) at the resonance tails, the computation with inhomogeneous broadening reproduces both the experimental peak and tails very well. Therefore, only the inhomogeneously broadened spectra explains the experiment accurately. Based on this analysis, our sample has 0.3 meV homogeneous and

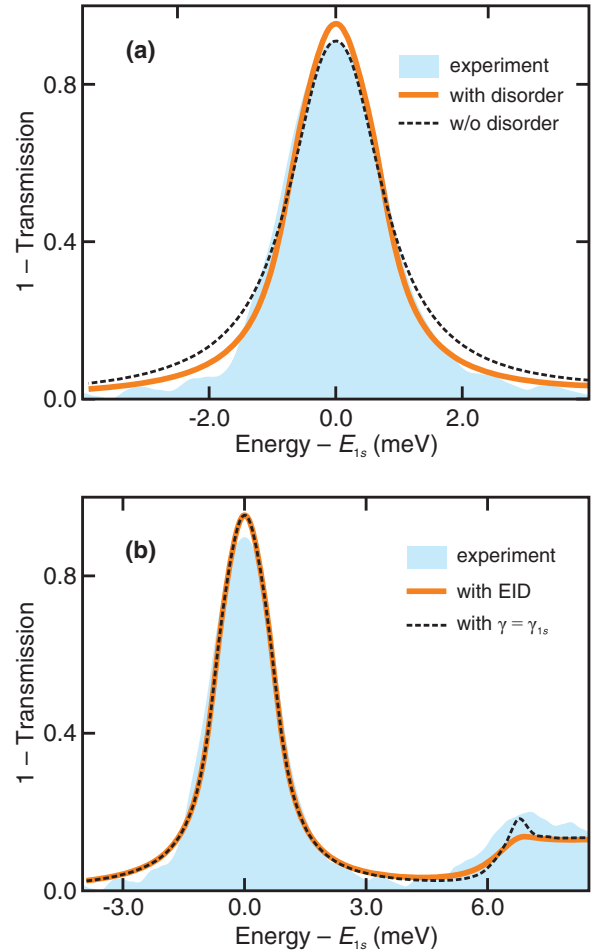


FIG. 3. (Color online) Experimental (shaded area) and theoretical (solid and dashed lines) spectra of $1 - T$ without THz field. (a) The results of the fully microscopic computation including EID are shown for inhomogeneous broadening (solid) versus homogeneous broadening (dashed). (b) Comparison of constant dephasing (dashed) versus EID (solid) when inhomogeneous broadening is included.

roughly 0.2 meV inhomogeneous broadening. These values are in good agreement with linewidth measurements [33,34] performed on comparable samples.

As a general trend, the EID broadens the $2s$ resonance much more than the $1s$ peak. This essential EID effect can be switched off in computations by setting all γ_λ to be equal to γ_{1s} . Figure 3(b) shows the computed $1 - T$ spectrum with (solid line, $\gamma_\lambda = 2\gamma_{1s}$) and without (dashed line, $\gamma_\lambda = \gamma_{1s}$) the EID effects as well as the measured spectrum (shaded area). We observe that the EID computation explains the experiment better than a constant- γ computation. More specifically, the computation without EID produces a too well-resolved $2s$ resonance compared with the strongly broadened $2s$ peak of the experiment. By matching the $2s$ width, we also know the EID-induced width of the other resonances, i.e., we use $\gamma_{\lambda \neq 1s} = \gamma_{2s} = 0.6$ meV based on Ref. [1].

Figure 3 very nicely shows that both inhomogeneous broadening and EID effects must be included to accurately describe our measurements. In the following, all computations have thus been performed using inhomogeneous broadening and

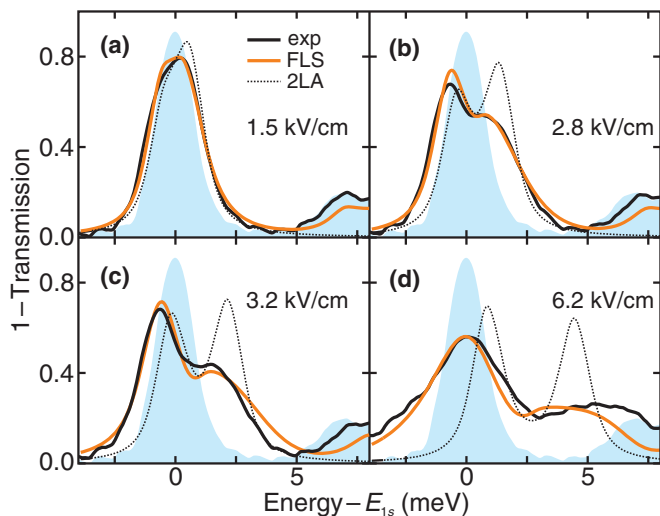


FIG. 4. (Color online) $1 - T$ without THz (shaded area) and with THz-photon energy of 6.8 meV, near the $1s-2p$ resonance, as measured in experiment (black solid), fully microscopic theory (orange solid), and the two-level result (dotted) for the THz-field strength of (a) 1.5 kV/cm, (b) 2.8 kV/cm, (c) 3.2 kV/cm, and (d) 6.2 kV/cm.

excitation-induced dephasing. The other material parameters are described in Ref. [13].

B. Full theory and two-level approximation for resonant and nonresonant excitation

Our detailed theory-experiment comparisons show that the full theory explains all experimentally observed features. As representative examples, we show in Fig. 4 spectra for selected THz-field strengths where the THz-photon energy is close to the $1s-2p$ resonance and in Fig. 5 for the case where the THz-photon energy is tuned below the resonance energy. Both figures present the direct comparison of the experimental data with THz (black solid) and the microscopic result (orange), i.e., using the full-level system (FLS). The experimental data without THz are shown as shaded areas; the results using the two-level approximation (2LA) are dotted.

The fully microscopic theory nicely reproduces the experimental results, including the peak heights, position, and THz-induced broadening. In contrast, the 2LA works only for the lowest THz field [Figs. 4(a) and 5(a)]. For higher THz field (2.8 kV/cm and higher), the 2LA becomes worse about the peak heights and broadening. For example, it overestimates the high-energy Rabi-peak height by 55% for 3.2 kV/cm THz-field strength for 6.8 meV THz-photon energy. However, it roughly describes the peak splitting correctly and the discrepancy of 2LA and experimental peak positions increases slightly with detuning.

To gain an overview of the dependence of THz-field strength and detuning on the Rabi peaks, we present in Figs. 6(b) and 6(d) the results for $1 - T$ as predicted by the fully microscopic theory for low (1.2 kV/cm) and medium THz-field strength (3.2 kV/cm), respectively. The experimental Rabi peaks are depicted as circles inside the contour plot, where the diameter refers to the peak height. We

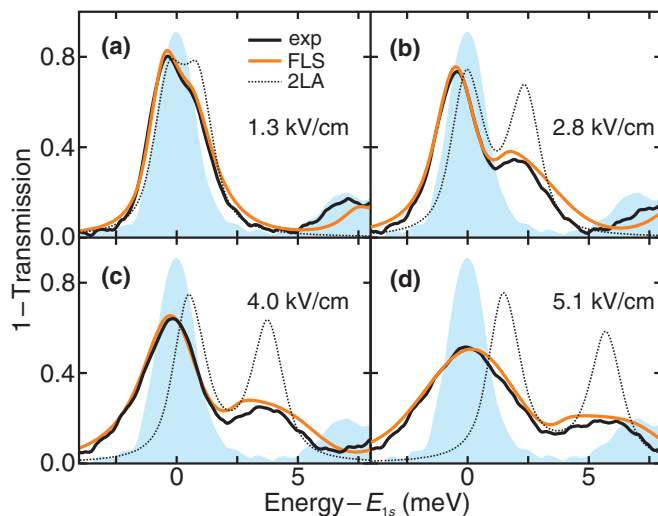


FIG. 5. (Color online) $1 - T$ without THz (shaded area) and with THz-photon energy of 6.2 meV, below the $1s-2p$ resonance, as measured in experiment (black solid), from the fully microscopic theory (orange solid), and the two-level result (dotted) for the THz-field strength (a) 1.3 kV/cm, (b) 2.8 kV/cm, (c) 4.0 kV/cm, and (d) 5.1 kV/cm.

observe that the Rabi splitting increases with the strength of the THz field as expected [25]. The spectra for the 2LA are presented in Figs. 6(a) and 6(c). For low THz field [1.2 kV/cm, Figs. 6(a) and 6(b)], the 2LA gives similar results as the microscopic theory. However, already for a medium THz field, the microscopic theory predicts asymmetric bleaching and

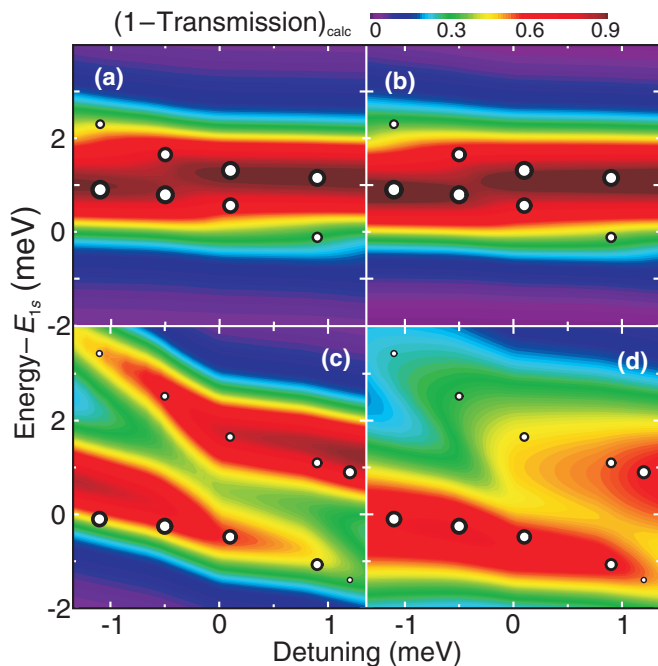


FIG. 6. (Color online) Anticrossing behavior of $1 - T$ extracted from the microscopic calculation. The experimental peak positions (heights) are depicted by the position (diameter) of the open circles. (a), (c) 2LA, and (b), (d) microscopic-theory results for a THz field of 1.2 (top) and 3.2 kV/cm (bottom).

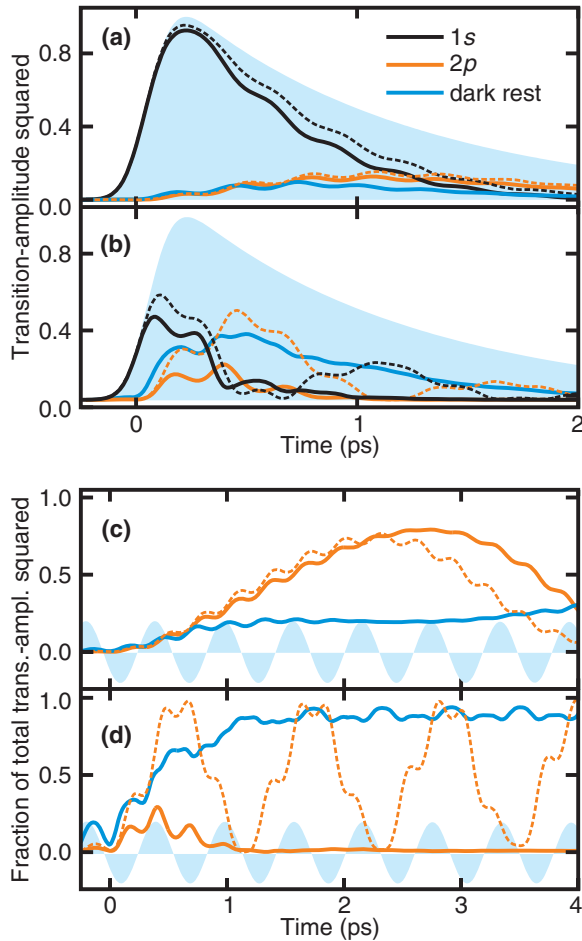


FIG. 7. (Color online) Top: The transition-amplitude squared for THz-photon energy near the $1s$ – $2p$ resonance. The THz-field strengths are (a), (c) 1.5 kV/cm, and (b), (d) 6.2 kV/cm. Shaded area: Sum of all squared transition-amplitudes without THz field. Solid (dashed) lines: microscopic (2LA) result with THz field. Bottom: $2p$ and the dark rest squared transition-amplitude as fraction of all squared transition amplitudes. Solid (dashed) lines depict microscopic (2LA) results. Shaded area: THz-field oscillations (arb. units). Note the difference in the time scales for the upper and lower panels.

broadening of the Rabi peaks in agreement with the experimental results [Fig. 6(d)], while the 2LA yields symmetric splitting and bleaching [Fig. 6(c)]. Hence, the observation of anticrossing is not enough to prove the validity of a 2LA. This shows the importance of higher excitonic states for the shapes of the $1s$ -exciton peak for medium THz fields leading to a complete disagreement of 2LA and experiment for high THz fields as already seen in Figs. 4(d) and 5(d).

The microscopic calculations allow us to follow the redistribution of existing THz polarization also in the time domain. Representatively, we analyze the temporal data for which the spectra were already shown in Figs. 4(a) and 4(d), for THz excitation near the $1s$ – $2p$ resonance. In Figs. 7(a)

and 7(b), the $1s$ squared transition amplitude $|p_{1s}|^2$ without THz is plotted as a shaded area as a reference. The results for the squared transition amplitude $|p_{\lambda}|^2$ from the microscopic theory with THz influence are shown in solid lines ($1s$: black; $2p$: orange; other dark states: blue). For comparison, we show the 2LA results as dashed lines. For the low THz intensity [1.5 kV/cm; see Fig. 7(a)], the microscopic theory and the 2LA basically agree. However, the microscopic calculation reveals that we already have a contribution from the squared transition amplitude of higher-lying exciton states. For high THz field [6.2 kV/cm; see Fig. 7(b)], we see only one Rabi flop in the microscopic calculation while the 2LA incorrectly predicts multiple Rabi flopping. To better monitor the THz influence, we replot the data for $2p$ and the dark states, but scaled as a fraction of all temporarily existing squared transition amplitudes. The results are shown in Figs. 7(c) and 7(d) for THz-field strengths of (c) 1.5 kV/cm and (d) 6.2 kV/cm. For illustration, the oscillating THz field is shown by the shaded area. For the low THz-field strength [Fig. 7(c)], the microscopic theory and the 2LA both describe $1s$ – $2p$ Rabi flopping. The Rabi period decreases with higher THz fields (intermediate fields not shown here) until for the highest THz field, all squared transition amplitude is immediately transferred into higher dark states [see blue line in Fig. 7(d)] while the 2LA incorrectly predicts continued Rabi flopping. Despite these limitations, however, the 2LA predictions of the Rabi splitting (determined by the Rabi period) are still quite correct.

V. CONCLUSIONS

We have measured the THz-induced changes in the optical transmission for a THz frequency near the excitonic $1s$ – $2p$ -transition frequency. We have observed bleaching and shifting of the $1s$ exciton peak and pronounced Rabi splitting. In addition, the Rabi peaks undergo an anticrossing behavior for a detuning of the THz frequency away from the exciton resonance. The fully microscopic theory excellently reproduces all experimental features and follows the transition from Rabi flopping at low THz intensities to exciton ionization at high intensities. We also have quantified how a restriction to only two levels (2LA) deviates from experiments and the fully microscopic theory. The 2LA works reasonably well for low THz fields where the Rabi splitting is weak. For elevated THz fields, only the Rabi-peak positions are rather close to experimental values while the peak heights are not reproduced. This systematic analysis closes the gap between earlier studies showing either dressed-state behavior for weak THz fields or THz ionization for strong and spectrally broad THz fields.

ACKNOWLEDGMENTS

We thank P. Michel, W. Seidel, and the FELBE team for their dedicated support. The Marburg work was supported by Deutsche Forschungsgemeinschaft. The Tucson group acknowledges support of NSF ERC CIAN and NSF AMOP.

[1] M. Kira and S. W. Koch, *Prog. Quantum Electron.* **30**, 155 (2006).

[2] R. A. Kaindl, M. A. Carnahan, D. Hagele, R. Lovenich, and D. S. Chemla, *Nature (London)* **423**, 734 (2003).

- [3] I. Galbraith, R. Chari, S. Pellegrini, P. J. Phillips, C. J. Dent, A. F. G. van der Meer, D. G. Clarke, A. K. Kar, G. S. Buller, C. R. Pidgeon, B. N. Mordin, J. Allam, and G. Strasser, *Phys. Rev. B* **71**, 073302 (2005).
- [4] R. Ulbricht, E. Hendry, J. Shan, T. F. Heinz, and M. Bonn, *Rev. Mod. Phys.* **83**, 543 (2011).
- [5] M. Jörger, T. Fleck, C. F. Klingshirn, and R. von Baltz, *Phys. Rev. B* **71**, 235210 (2005).
- [6] R. Huber, B. A. Schmid, Y. R. Shen, D. S. Chemla, and R. A. Kaindl, *Phys. Rev. Lett.* **96**, 017402 (2006).
- [7] J. R. Danielson, Y.-S. Lee, J. P. Prineas, J. T. Steiner, M. Kira, and S. W. Koch, *Phys. Rev. Lett.* **99**, 237401 (2007).
- [8] M. Kira and S. W. Koch, *Phys. Rev. Lett.* **93**, 076402 (2004).
- [9] G. Khitrova, H. M. Gibbs, M. Kira, S. W. Koch, and A. Scherer, *Nat. Phys.* **2**, 81 (2006).
- [10] M. Wagner, H. Schneider, D. Stehr, S. Winnerl, A. M. Andrews, S. Scharfner, G. Strasser, and M. Helm, *Phys. Rev. Lett.* **105**, 167401 (2010).
- [11] K. Johnsen and A.-P. Jauho, *Phys. Rev. Lett.* **83**, 1207 (1999).
- [12] D. S. Citrin, *Phys. Rev. B* **60**, 13695 (1999).
- [13] A. Liu and C.-Z. Ning, *J. Opt. Soc. Am. B* **17**, 433 (2000).
- [14] J. T. Steiner, M. Kira, and S. W. Koch, *Phys. Rev. B* **77**, 165308 (2008).
- [15] A. V. Maslov and D. S. Citrin, *Phys. Rev. B* **62**, 16686 (2000).
- [16] X. W. Mi, J. C. Cao, and C. Zhang, *J. Appl. Phys.* **95**, 1191 (2004).
- [17] T. Y. Zhang, W. Zhao, X. M. Liu, and C. Zhang, *Appl. Phys. Lett.* **91**, 041909 (2007).
- [18] J.-Y. Yan, R.-B. Liu, and B.-f. Zhu, *New J. Phys.* **11**, 083004 (2009).
- [19] B. Ewers, N. S. Köster, R. Woscholski, M. Koch, S. Chatterjee, G. Khitrova, H. M. Gibbs, A. C. Klettke, M. Kira, and S. W. Koch, *Phys. Rev. B* **85**, 075307 (2012).
- [20] M. Wagner, M. Teich, M. Helm, and D. Stehr, *Appl. Phys. Lett.* **100**, 051109 (2012).
- [21] G. M. H. Knippels, X. Yan, A. M. MacLeod, W. A. Gillespie, M. Yasumoto, D. Oepts, and A. F. G. van der Meer, *Phys. Rev. Lett.* **83**, 1578 (1999).
- [22] T. Grunwald, T. Jung, D. Köhler, S. W. Koch, G. Khitrova, H. M. Gibbs, R. Hey, and S. Chatterjee, *Phys. Status Solidi C* **6**, 500 (2009).
- [23] H. Haug and S. W. Koch, *Quantum Theory of the Optical and Electronic Properties of Semiconductors*, 5th ed. (World Scientific, Singapore, 2009).
- [24] C. N. Böttge, S. W. Koch, L. Schneebeli, B. Breddermann, A. C. Klettke, M. Kira, B. Ewers, N. S. Köster, and S. Chatterjee, *Phys. Status Solidi B* **250**, 1768 (2013).
- [25] M. Kira and S. W. Koch, *Semiconductor Quantum Optics*, 1st ed. (Cambridge University Press, Cambridge, England, 2011).
- [26] M. Kira, F. Jahnke, W. Hoyer, and S. W. Koch, *Prog. Quantum Electron.* **23**, 189 (1999).
- [27] H. Wang, K. Ferrio, D. G. Steel, Y. Z. Hu, R. Binder, and S. W. Koch, *Phys. Rev. Lett.* **71**, 1261 (1993).
- [28] T. Rappen, U.-G. Peter, M. Wegener, and W. Schäfer, *Phys. Rev. B* **49**, 10774 (1994).
- [29] P. Borri, W. Langbein, J. M. Hvam, and F. Martelli, *Phys. Rev. B* **59**, 2215 (1999).
- [30] B. Mieck, H. Haug, W. A. Hügel, M. F. Heinrich, and M. Wegener, *Phys. Rev. B* **62**, 2686 (2000).
- [31] W. Schäfer, R. Lövenich, N. A. Fromer, and D. S. Chemla, *Phys. Rev. Lett.* **86**, 344 (2001).
- [32] C. N. Böttge, Ph.D. thesis, Philipps-Universität Marburg, Marburg, Germany, 2013.
- [33] S. T. Cundiff, *J. Opt. Soc. Am. B* **29**, A69 (2012).
- [34] M. E. Siemens, G. Moody, H. Li, A. D. Bristow, and S. T. Cundiff, *Opt. Express* **18**, 17699 (2010).